


Modeling of the effectiveness of novel edge seal designs for fast, low-Cap-Ex manufacturing

Michael D. Kempe¹  | Alliston Watts¹ | Tushar Shimpi² | Samuel Ellis² | Kurt Barth³

¹National Renewable Energy Laboratory (NREL), Golden, Colorado, USA

²Next Generation Photovoltaics Center, Colorado State University, Fort Collins, Colorado, USA

³Centre for Renewable Energy Systems Technology, Wolfson School of Mechanical, Electrical and Manufacturing Engineering, Loughborough University, Loughborough, UK

Correspondence

Michael D. Kempe, National Renewable Energy Laboratory (NREL), 15013 Denver West Pkwy, Golden, CO 80401, USA.
Email: michael.kempe@nrel.gov

Funding information

US Department of Energy,
Grant/Award Number: DE-EE-0008161 0

Abstract

In the manufacturing of photovoltaic (PV) modules, the lamination process can take up to 20 min to complete. In this work, new lamination processes are being developed, and have been prototyped, which hope to be able to cut this time down to as little as 30 s. This could provide significant savings in the cost of lamination equipment, floor space, and energy. PV modules are expected to have a lifespan exceeding 20 to 30 years. For moisture-sensitive PV technologies, the edge seal between the two layers of glass can be the weakest point of its reliability. There is an inherent challenge when evaluating edge seal materials due to their low permeation rates. As part of Colorado State University's Photovoltaic Research and Development 2, work at the National Renewable Energy Laboratory has developed models to evaluate edge seal configurations in glass-glass PV modules. Here, this new manufacturing process is evaluated for long-term moisture durability. Different edge seal design options within glass-glass PV modules are explored. Most of these designs are targeting a superstrate on glass configuration, e.g CdTe, but some designs could be used on conventional crystalline Si cells. Using COMSOL finite element simulation software, we investigated the edge seal and interlayer design configurations containing silicone perimeter edge adhesive, desiccated polyisobutylene-based edge seal, air, and polyolefin while integrating climate conditions equivalent to a hot and humid environment such as Miami, Florida. We found optimized configurations that will allow the module to prevent moisture ingress over 50 years minimizing the amount of time and material used while utilizing polymers that are easily dispensed.

KEYWORDS

desiccant, diffusion, edge seal, lamination, moisture, packaging

This is an open access article under the terms of the Creative Commons Attribution License, which permits use, distribution and reproduction in any medium, provided the original work is properly cited.

© 2023 Alliance for Sustainable Energy, LLC and Colorado State University. *Energy Science & Engineering* published by Society of Chemical Industry and John Wiley & Sons Ltd.

1 | INTRODUCTION

In the manufacturing of photovoltaic (PV) modules, one of the last steps is the vacuum lamination process. Typically, this process takes about 8 min to 12 min¹ and is primarily limited by the time it takes to heat up the module to temperatures above about 135°C, where the peroxide curing agent, *tert*-butylperoxy 2-ethylhexyl carbonate, can be substantially decomposed to provide adequate crosslinking of the encapsulant. Because of the potential to create other problems caused by excessive heat, one cannot simply use a laminator bed with a higher temperature.

To overcome this issue, institutions such as Abound Solar,^{2,3} Apollon Solar,^{4–7} and the Next Generation Photovoltaic Center at Colorado State University^{8,9} have developed significantly faster lamination processes that do not use vacuum lamination. Instead, these processes use various forms of atmospheric pressure lamination with two glass plates using an edge seal/adhesive around the perimeter and various attachment adhesives in the center area.

These methods result in air gaps which when using crystalline Si cells create two additional air-to-solid material interfaces with higher reflectivity. This has been addressed by Apollon Solar through the use of specialized antireflective coatings.⁷ But for superstrate thin films, such as CdTe, this optical coupling is not a concern. Additionally, the presence of an air gap does reduce heat transfer. However, the primary resistance to heat transfer is the convective transfer to the environment such that the average effect is less than about 0.5°C when modules are operating at 15°C to 20°C above ambient.³

In this work, the silicone polymeric adhesives are dispensed at room temperature, but the polyisobutylene (PIB) edge seal or the encapsulant is dispensed at temperatures high enough to be well past melting transitions where the viscosity is sufficiently low. Because the glass is not heated up to the cure temperature, the limitation to processing speed is determined by the mechanical speed and number of extrusion heads. Depending on the specifics of the process, this can result in processing times as low as 30 s and/or reductions in floor space by up to a factor of five,⁴ along with a significant reduction in capital expenditures.

PV devices are exposed to a variety of climates and weather conditions and are intended to last for at least the typical warranty period of 25 or more years.^{10,11} In particular, many thin film materials have higher relative sensitivities to moisture than do crystalline Si technologies.^{12–19} In glass–glass modules, a key factor for the life

expectancy is dependent on its ability to reduce the moisture absorbed through its edges.²⁰ Reduction of moisture ingress through the internal components is dependent on the edge seal composition, amount of desiccant, and the width of each component layer. In particular, PIB-based materials have proven to be extremely effective at preventing moisture ingress.^{18,21–23} This investigation focuses on the glass–glass edge seal configurations with two variations within the interlayer: discrete interlayer components and a fully covered interlayer. Both interlayer options present unique features that can be beneficial when reducing moisture. These designs are suitable for thin film superstrate configurations, but some are also suitable for crystalline Si or for substrate-based thin film designs such as a copper indium gallium selenide (CIGS) device.

2 | EXPERIMENTAL METHODS

2.1 | Diffusivity and solubility measurement

Determining how long it takes for water to enter a module requires knowledge of the diffusivity and solubility of the packaging materials. Films of a black oxime condensation cure polydimethyl siloxane (PDMS) adhesive (Tosan 1527) were made by placing it between two release liners and two rigid plates with spacers between the release liners to control the thickness at 1.1, 3.1, and 4.8 mm. This was left for a few weeks to make sure moisture could permeate the package to cure the material before removing the release liners. A film of Helioclear 107 was made by pressing it in a heated press at 140°C to thicknesses of 0.9 and 1.5 mm. These films were cut into 12-cm-diameter films to allow the transient water vapor transmission rate (WVTR) to be measured using a Mocon Permatran-W 3/31 instrument. For the silicone, thick films were necessitated by the high diffusivity, which, for the 50-cm² cross-sectional area of the Mocon test cell and a flow of 200 SCCM of nitrogen, was sometimes above the operational range of the instrument (0.07–200 g/m²/day). The Mocon was also equipped with a remote test cell inside of an ESPEC (Model SH-641) environmental chamber that allowed temperatures between 10°C and 85°C to be reached at 0% to 100% relative humidity (RH).

The transient WVTR was measured by first drying the films in the Mocon test cell by blowing dry nitrogen separately over the top and bottom of the film until moisture was no longer detected. Then, liquid water was injected into the bottom chamber. Alternatively, the humidity was introduced by placing the sample in the

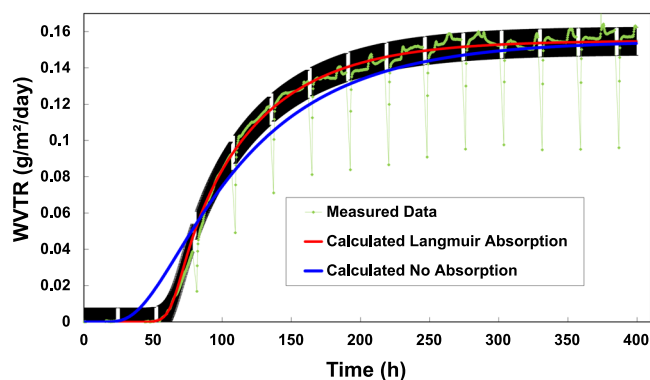


FIGURE 1 Sample water vapor transmission rate (WVTR) measurement was used to measure diffusivity. Helioseal 107 polyisobutylene (PIB). $T = 30^{\circ}\text{C}$; 0.9 mm thick. The *blue* line was calculated using Equation (1). The *red* line was calculated using a numerical solution with a Langmuir absorption isotherm, Equation (2), which models the absorption capability of the particle surface as having a limited total surface area and holding capacity, K_1 , and a factor, K_2 , accounting for the ability to reach saturation as a function of the absorbed water concentration C . The black band represents an uncertainty equal to $\pm 5\%$ of the steady state WVTR as a reasonable fit criterion.

humidity-controlled ESPEC chamber and humidified air was pulled in by pulling out air with a pump. This allows the transient WVTR to be measured, Figure 1. There is also a small ~ 80 s instrumental lag requiring the data to be shifted accordingly. Assuming Fickian diffusivity (i.e., diffusivity is independent of concentration), and no absorption of water on filler particles, the transient WVTR can be described by

$$WVTR = \frac{DC_s}{l} \left[1 + 2 \sum_{n=1}^{\infty} (-1)^n e^{\left(\frac{-Dn^2\pi^2 t}{l^2} \right)} \right], \quad (1)$$

where D is diffusivity, C_s is saturation concentration, t is time, and l is sample thickness.²⁴ The diffusivity is first determined by the time required to reach a steady state, after which the water saturation concentration is determined by the steady-state WVTR for a Fickian material.

For both the silicone and the PIB, the transient WVTR curve could not fit well with the measured data. The setup we used should be able to produce a curve that matches the predicted curve, Equation (1), within $\pm 5\%$ as shown in Figure 1. While neither of these materials has desiccant intentionally added to it for the purpose of slowing water ingress, they both demonstrate a behavior that can be interpreted as an adsorbing desiccant. That is, the initial lag time is too long considering the abruptness with which water approaches the steady-state value. Both materials have filler materials added to them to modify

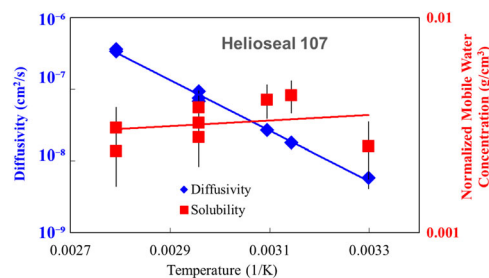


FIGURE 2 Diffusivity and solubility results for Helioseal 107. For the 85°C data, the 50% relative humidity (RH) solubility data were doubled to make them equivalent to the 100% RH data point.

the rheological properties to aid in processing them and for the intended application. These inorganic fillers can absorb water on the surface, but in a reversible manner. To model the adsorption, we chose to use a Langmuir isotherm

$$A = K_1 \left[\frac{K_2 C}{1 + K_2 C} \right], \quad (2)$$

which models the absorption capability of the particle surface as having a limited total surface area and holding capacity, K_1 , and a factor, K_2 , accounting for the ability to reach saturation as a function of the absorbed water concentration in the polymer matrix, C .

With the use of the Langmuir isotherm, we do not have a simple analytical solution for the transient WVTR. Therefore, a visual basic program was made to calculate a numerical solution with the assumption of Fickian diffusion in the polymer (Figure 1). A one-dimensional model was used with water divided between an immobilized fraction and a mobile fraction at each node. The mobile fraction diffuses at each time step in accordance with Fick's law and the immobile fraction is equilibrated according to Equation (2) at the end of each time step. For each material, the value of K_1 was fixed for all temperatures and RH settings. This is in effect assuming that the effective area for moisture absorption is constant. Then, K_2 is determined at each temperature quantifying the affinity for the absorption sites as a function of temperature. In total, there are four fitting parameters for each material measurement, K_1 for all temperatures and humidities, and a value of K_2 , D , and S for each temperature/humidity measurement. The diffusivity, solubility, and K_2 results for Helioseal 107 are shown in Figures 2 and 3 respectively.

For both the Helioseal 107 and Tonsan 1527 materials, measurements were made as a function of temperature at 100% RH. A lower humidity measurement of 50% RH was also made at 85°C . For the purposes of modeling, the solubility, C , was assumed to be a linear

function of humidity with an Arrhenius dependence on temperature, T , as

$$C = RH \times C_0 e^{-\frac{Ea_S}{RT}}, \quad (3)$$

where C_0 is a prefactor with units of g/cm^3 , Ea_S is the solubility activation energy, R is the universal gas constant, and RH is expressed as a fractional value. Here, water is assumed to be in equilibrium between two states, one immobilized and adsorbed on the surface of filler materials, and the other free to diffuse throughout the material. The value of C in Equation (3) only refers to water in the mobile phase. In this model, we are ignoring the fact that diffusion cannot happen through the filler particles, which means that the diffusion constant, D , is an effective diffusion constant. We also assume that diffusivity conforms to an Arrhenius thermal acceleration according to

$$D = D_0 e^{-\frac{Ea_D}{RT}}, \quad (4)$$

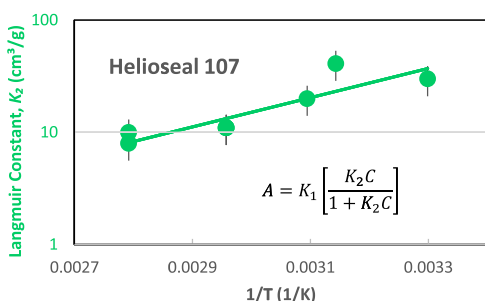


FIGURE 3 Langmuir constant, K_2 , as a function of inverse temperature for Helioseal 107.

where D_0 is a prefactor with units of cm^2/s and Ea_D is the activation energy for diffusion. Similarly, the Langmuir equilibrium constant, K_2 , is thermally activated and was similarly modeled using an Arrhenius function

$$K_2 = K_{20} e^{-\frac{Ea_{K_2}}{RT}}, \quad (5)$$

where K_{20} is the Arrhenius prefactor and Ea_{K_2} is the activation energy for the Langmuir equilibrium constant. The Arrhenius fit parameters and K_1 are provided in Table 1.

Some of the models use a desiccated PIB model for which the modeling parameters were obtained from Kempe et al.²² and are indicated in Table 1. Other models utilized small air gaps for which the diffusivity and vapor concentration parameters were obtained from an Arrhenius fit utilizing a data set between 0°C and 100°C.

Some of the models utilize an interlayer polyolefin material which has not been selected yet. Therefore, we developed generic parameters based on typical values for permeation parameters of polyolefin encapsulants used in the PV industry. This other data set had values of 44.3 ± 3.8 and 23.2 ± 5.8 kJ/mol for the activation energy of diffusivity and solubility from which rounded-off values of 45 and 25 kJ/mol were chosen, respectively. Next, the Arrhenius prefactors were adjusted to yield typical values at 25°C for diffusivity and solubility. Not having precise values for this material does introduce some uncertainty in the correlation of the models to an actual module. It should be remembered that these materials are subject to being substituted for others in the future. The material model parameters in Table 1 are more accurately regarded in the context of this paper as representative values for these parameters.

TABLE 1 Values for water permeation parameters in various mediums.

		Silicone adhesive (aka, Tonsan 1527)	PIB edge seal (aka, Helioseal 107)	Desiccated PIB edge seal ²²	Air	Interlayer PO material (estimated typical)
Diffusivity parameters	Ea_D (kJ/mol)	30.3	67.6	54.8	6.66	45
	D_0 (cm^2/s)	0.269	2360	17	3.52	36.8
	D at 45°C (cm^2/s)	2.84×10^{-6}	1.85×10^{-8}	4.66×10^{-8}	0.284	1.50×10^{-6}
Solubility parameters	Ea_S (kJ/mol)	8.22	-2.49	5	40.4	25
	C_0 (g/cm^3)	0.0918	0.00131	0.0326	278	5.10
	C at 45°C and 25% RH (g/cm^3)	0.00103	0.000839	0.000632	0.0000159	0.000100
Langmuir constant	Ea_{K_2} (kJ/mol)	21.6	-25.0			
	K_{20} (cm^3/g)	161,000	0.00183			
Maximum immobilized water	K_1 (g/cm^3)	0.00065	0.00030	0.032		

Abbreviation: PIB, polyisobutylene; PO, polyolefin; RH, relative humidity.

3 | FINITE ELEMENT MODELING

We simulated 10 module designs, fabricated from two types of interlayers: Figure 4A,B, the discrete interlayer, and Figure 4C, the fully covered interlayer. The discrete interlayer internal area is comprised of 6-mm-wide ribbing, each 100 cm in length, with air in between the spaces. The ribbing is in some cases composed of desiccant-filled material. Because of the very high diffusivity of water in air, moisture is absorbed nearly equally by any strip of material in the gap. With ribbing, we are reducing the amount of material used, thus lowering the material cost reducing the time and equipment costs associated with the application of the interlayer. The ribbing is very quickly extruded through a nozzle at high temperatures to facilitate good adhesion without the requirement of fully heating up the glass plate. This design uses precise control over material volume and the material is easily pressed to the desired thickness.

Unlike the discrete interlayer, the full interlayer completely covers the internal module layer (Figure 4C). With the whole back area filled, there is a small improvement in thermal performance dropping the cell temperature by between 0.5°C and 1°C.³ The intent is to apply the layer by direct extrusion onto the plate bypassing the step of forming a separate film to be used in a vacuum lamination process. This would significantly reduce the amount of time and capital equipment necessary to assemble this type of module providing a large reduction in module assembly-related costs.

While the initial development of this novel design was for CdTe-based devices,^{2,3,8,9} the use of a fully filled interlayer can enable the use of crystalline Si-based cells but the difficulties associated with applying Si cell strings without significant cell cracking have not yet been developed. The reflection at interfaces will affect the performance by reducing transmitted light by about 8% just over the effective area of the bubbles. This sort of concept has been explored in the past by Evergreen solar,²⁵ and by Dow Corning with PDMS gels.^{26–30} PDMS and some of the materials used by Evergreen suffer from being inherently more expensive than polyolefinic encapsulants, but the reduced capex and cycle time may compensate for this shortcoming while providing for a low viscosity material that would not damage the crystalline Si cells when applied.

Both types of interlayer models are enclosed with 6 mm silicone and 6 mm PIB around the perimeter. The presence of a quaternary carbon in the PIB backbone stabilizes tertiary carbon radicals, making the polymer highly prone to chain scission, limiting the options for crosslinking chemistry. Consequently, PIBs tend to experience a reduction in molecular weight as they age. Because of this, the sparsely crosslinking, or uncrosslinked, PIBs used in PV applications will typically fail cohesively at very low values making them not useful to be relied upon for mechanical strength.^{31,32} To overcome this concern, the silicone perimeter layer is used to provide mechanical integrity. Here, it should be noted that the shear forces on a glass/glass construction PV module are small enough that even when an EVA is

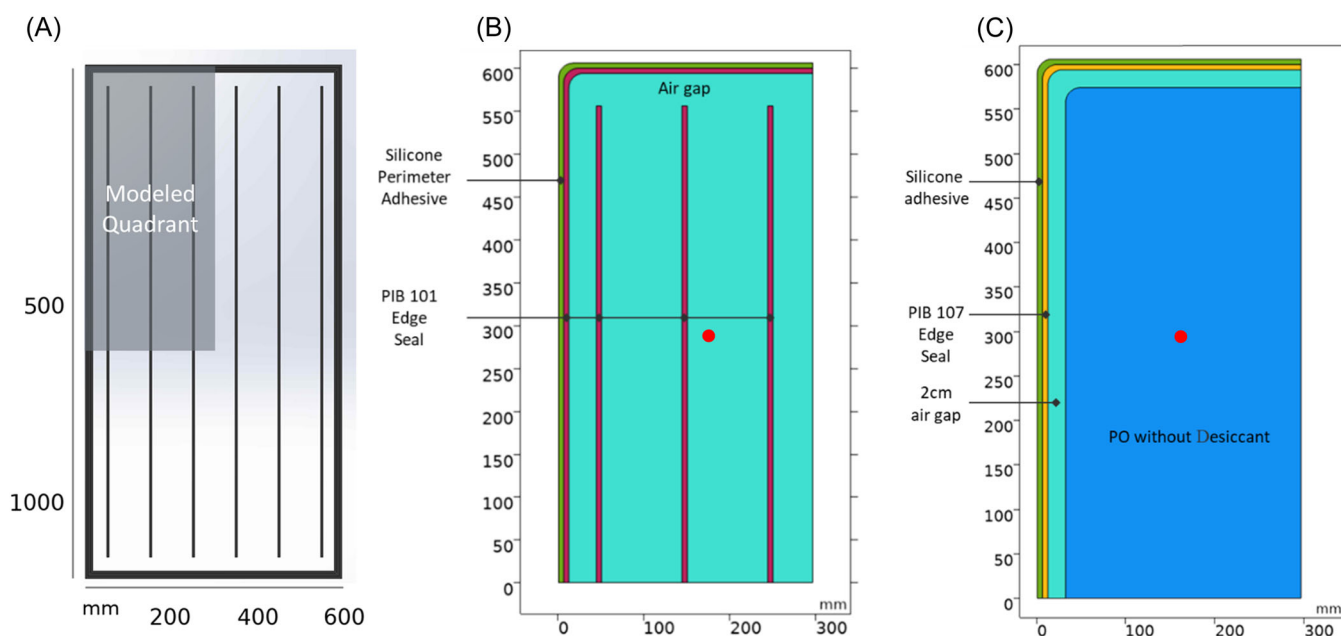


FIGURE 4 Schematic drawing of two types of designs. Comparison of the humidity over time was made for each model at the point located at a 300 mm from the top, and 150 mm from the side, indicated by the red dot, see Figure 15. (A) Full module construction. (B) Model #1 design with a discrete interlayer. Modeled quadrant only. (C) Model #9 with a filled interlayer. Modeled quadrant only.

formulated without a crosslinker and no frame is used, very little creep is observed.^{33,34} Just a small amount of durable silicone on the perimeter, especially when used in conjunction with a frame, is expected to be sufficient to prevent creep in the polymer interlayer.


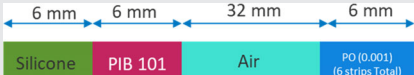
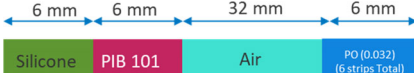
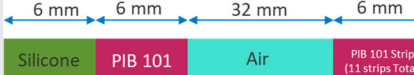
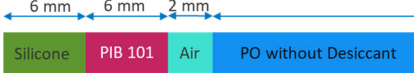



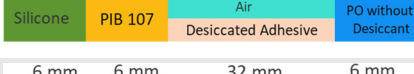
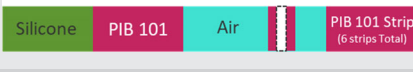
The simplified schematics of the 10 designs are shown below giving detail into the nature of the perimeter region, Table 2. For the interior, the interlayer models are shown in Figure 4. For the ribbing-containing models, either 6 lines are used as shown in Figure 4, or 11 similar lines with additional ribs placed between the existing ribs. The development of the processes to do the actual module assembly will be published elsewhere.

The moisture ingress through the edge of the module was simulated using COMSOL 5.4 with the Transport of Diluted Species module. The COMSOL model was developed from a non-Fickian Excel model³⁵ for the purpose of determining moisture ingress lifetime expectancy of new edge seal fast lamination application process for glass-to-glass modules. This COMSOL model is used to compute the diffusion and concentration through the two-dimensional (2D) interface in the PV module. The geometry is taken from a quarter section of

a 600 mm × 1200 mm glass/glass module as shown for Models #1 and #9 in Figure 4. The modules are assumed to be initially completely dry so that moisture diffuses from the exterior edges of the silicone, to the PIB edge seal, and into the interlayer. Due to the impermeability of the glass, a 2D model can be assumed for all but Model #9.

The outer exterior edge interface of the 2D model was assumed to be at equilibrium with both the temperature and RH of the exterior environment. The COMSOL program was designed to import temperature and RH data from a *.txt file to run the external equilibrium calculations and to estimate the permeation parameters. The solutions were generated with a time-dependent study ranging from 25 to 50 years with a 1-year step for data output. However, in the context of this work, a constant steady state value of 45°C and 25% RH was used. In previous work by Kempe et al.,²² it was found that the moisture ingress characteristics of PIB-based edge seals in Miami, Florida can be approximated by this condition. This approximation was taken because it is slightly easier and is equivalent. Because the time scale for ingress is many years, the detailed actual

TABLE 2 Design schematics for modules.

No.	Module schematic	Module construction description
1		PDMS and PIB 101 edge seal with six 100-cm-long and 6-mm-wide PIB 101 strips evenly space between the long sides of the module.
2		PDMS and PIB 101 edge seal with six 100-cm PO strips desiccated with 0.001 g/cm ³ evenly space between the long sides of the module.
3		PDMS and PIB 101 edge seal with six 100-cm PO strips desiccated with 0.032 g/cm ³ evenly space between the long sides of the module.
4		PDMS and PIB 101 edge seal with eleven 100-cm PIB strips evenly space between the long sides of the module.
5		PDMS and PIB 101 edge seal with a 2-mm air gap and PO without desiccant in the interlayer.
6		PDMS and PIB 101 edge seal with a 2-mm air gap and PO with 0.0001 g/cm ³ desiccant on the interlayer.
7		PDMS and PIB 101 edge seal with a 2-mm air gap and PO with 0.001 g/cm ³ desiccant on the interlayer.
8		PDMS and PIB 107 edge seal with a 2-mm air gap and PO without desiccant on the interlayer.
9		PDMS and PIB 107 edge seal with a 2-cm band of desiccated adhesive with an air gap on top. Model as air with 1/2 the solubility and with desiccant able to absorb 0.05 g/cm ³ .
10		PDMS and PIB 101 edge seal with six 100-cm-long and 6-mm-wide PIB 101 strips evenly space between the long sides of the module. A J-box hole opening was included on the interlayer.

Abbreviations: PDMS, polydimethyl siloxane; PIB, polyisobutylene.

meteorological data would only serve to put yearly fluctuations on top of the output plots in this work.

The values for the external equilibrium constants and for the permeability constants were obtained using the values in Table 1 with the associated equations. For the silicone and for PIB 107, the reversible equilibration between the adsorbed and immobilized water was modeled with the transport of diluted species interface. The initial conditions were set at the silicone-to-air boundary, surrounding the edge of the PV module. The outside perimeter conditions were derived from the equilibrium concentration in Equation (3), which is a function of the temperature and humidity. The right and bottom edges of the model in Figure 4 are symmetrical and can thus be modeled as a no-flux boundary.

Within most materials, water is modeled as existing in two states, a mobile and an immobilized state. This was modeled as two separate species in the same material with reactions enabling the conversion from one water species to another.

For reactive, irreversible species, this was accomplished as a series of if-then statements. Because time steps are discrete and the fact that a reaction rate, not net mass transfer, must be specified, there is the possibility for this to overload the irreversible desiccant. To fix this, the if-then statements allowed for reverse “reactions” when the desiccant was overloaded.

For the Langmuir-modeled desiccants, the reaction between the two modeled water species was modeled as a reaction rate proportional to the difference in equilibrium between the two states. This will allow for moisture to move back and forth between adsorbed and mobile water, always heading toward equilibrium.

At the interfaces between materials, it is the chemical potential of water that is constant, not the concentration. This can also be represented by the RH of water in the two mediums. At interfaces, the mass flux of water must also be conserved. This is handled by an inward flux (j_{c1}) boundary condition in domain 1 for the first material at concentration (C_1)

$$j_{c1} = M \left(C_1 - \frac{C_{1,\text{sat}}}{C_{2,\text{sat}}} C_2 \right), \quad (6)$$

and in domain 2 of the second material with a flux (j_{c2}) and concentration (C_1) given by

$$j_{c2} = M \left(\frac{C_{1,\text{sat}}}{C_{2,\text{sat}}} C_2 - C_1 \right), \quad (7)$$

where M is a mass transfer coefficient with units of [m/s], and $C_{1,\text{sat}}$ and $C_{2,\text{sat}}$ are the saturation of water in domains 1 and 2, respectively at 100% RH. A value of $M = 1$ m/s was

used. These equations do not explicitly keep the concentration at the correct value but instead force a conservation of mass while forcing the concentration to be continually moving toward the correct equilibrium point.

4 | MODELING RESULTS

4.1 | Model #1

This model design is shown in detail in Figure 4B and is very similar to the construction Abound Solar used for their CdTe modules with 6 mm of silicone and 6 mm of desiccant containing edge seal at the perimeter,^{2,3} but with fewer ribs placed in the center area of the module. Figure 5A,B shows us the model results for the mobile water concentration, in g/cm³, on a line from the edge of the module toward the center. The moisture profile in the silicone (outer 6 mm perimeter) is nearly flat because its diffusivity is so high relative to PIB 101. Then, at the silicone to PIB 101 interface, there is a discontinuity in the mobile water concentration because it is the chemical potential of water in the polymer that is constant across a membrane, not the concentration. The diffusivity in PIB 101 is so small that almost all the concentration drop occurs here. Conversely, in air, the diffusivity is orders of magnitude higher than that in silicone, creating a concentration gradient in the air that is nearly flat (Figure 5D). Even in the center of the module where the total diffusion length is around a meter as opposed to a few centimeters, the moisture concentration in the air is essentially the same everywhere. This can be understood in the context that the characteristic equilibration time (τ) is related to diffusivity by the square of the characteristic distance (X_c) as

$$\tau = \frac{X_c^2}{D}, \quad (8)$$

As shown in Table 1, the diffusivity in air is $\sim 10^7$ times higher than that in PIB such that the factor $\sim 100^2 = 10^4$ attributable to the longer distance is irrelevant and the concentration in the air is essentially always at equilibrium on the relevant timescales of this model.

After the moisture diffuses through the silicon, in a matter of minutes, it then takes approximately 10 years to get through the PIB 101 edge seal where it can diffuse laterally in the 2D plane to the desiccated strips. The solubility of mobile water in the PIB is greater than its concentration in air at the same RH creating a discontinuous increase in concentration going from air to PIB. Because water is immobilized by the desiccant of the PIB, it must first consume the desiccant at the perimeter of the strips. Therefore, water is only present at

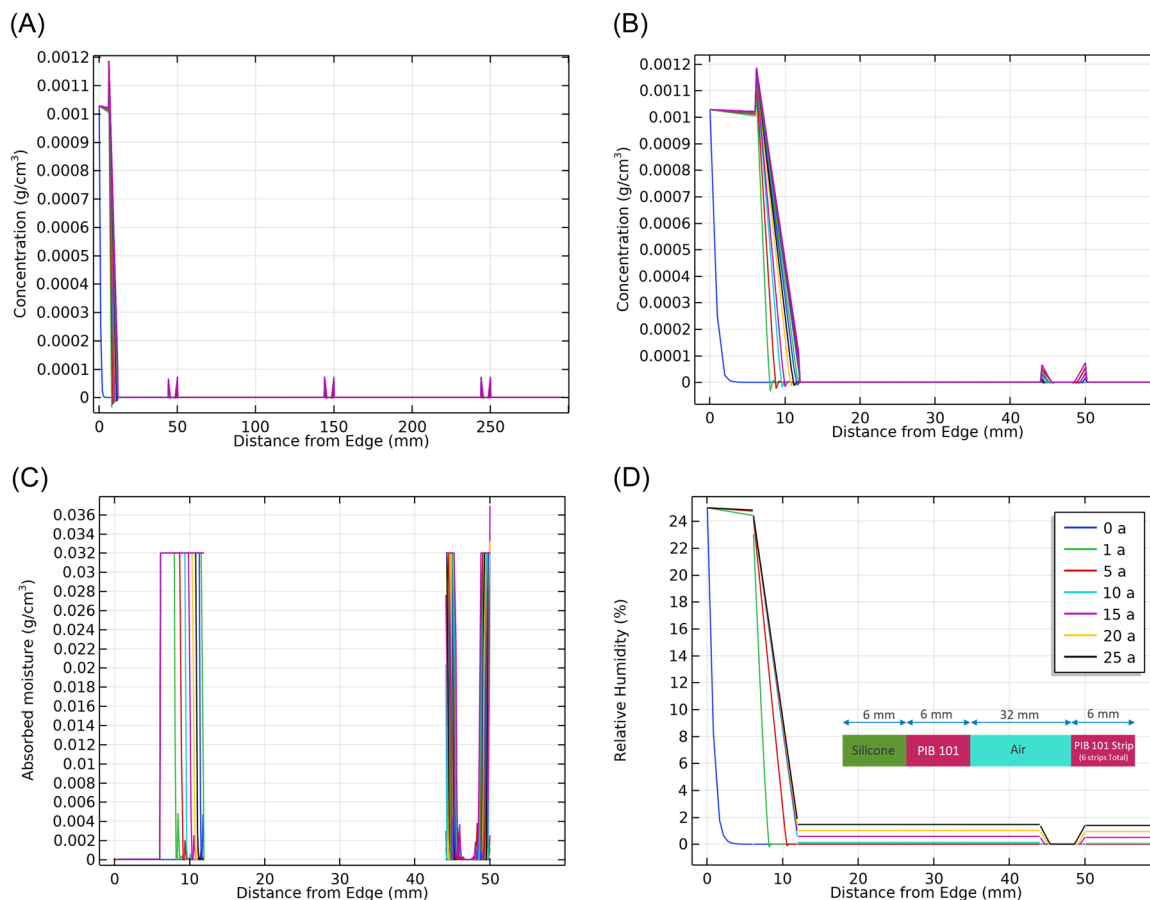


FIGURE 5 Model option #1, the discrete interlayer is as shown in Figure 4B, but the concentration is plotted up to the 300 mm distance from the edge of the module to the center starting at a midpoint on the longer edge. (A) Mobile water concentration. (B) Close-up plot of water concentration. (C) Absorbed moisture profile. (D) Relative humidity profile. The legend in (D) shows the line color that corresponds to the year in the simulation.

the sides of the ribbing producing spikes in the concentration at 50 mm, 150 mm, and 250 mm distances. The spikes are nearly triangular in shape as the concentration goes from an increasing equilibrium value with the air down to zero at the point where there is unreacted desiccant. This profile is nearly a straight line because the concentration of mobile water in the PIB at 25% RH is 26× lower than immobilized water (Figure 5B). Furthermore, at its maximum, the RH in the air gap only reaches ~1.8%, making this ratio always higher than about 360×. This means that the front for the unreacted desiccant moves extremely slowly and is well approximated by a quasi-steady state solution.

The profile for absorbed, immobilized moisture is a progression of widening squared peaks instead of triangular spikes (Figure 5C). In the PDMS perimeter, the amount of absorbed moisture is so much smaller than in PIB 101 that it is not visible in the plot. This profile first progresses through the perimeter PIB till it reaches the air space, and then begins to progress through the PIB ribbing. This is because there is

essentially a front with unreacted desiccant on one side and consumed desiccant on the other side. The inability of water to reach the center of the strips is due to the low diffusivity of the PIB. A higher diffusivity is desirable in a matrix containing desiccant that is intended to be consumed over its lifetime.

The profile for the evolution of the RH follows a much more intuitive progression (Figure 5D), monotonically decreasing till it reaches the center of the ribbing. While this design (Model #1) does significantly lower the RH in the module, there is still ~1.8% RH expected to be present at the end of life of the module, which, depending on the technology, may affect its performance.

4.2 | Model #2

To overcome the inability of the desiccant to be fully utilized in the ribbing, this model utilizes a PO matrix with a much higher, ~32×, diffusivity than PIB 101.

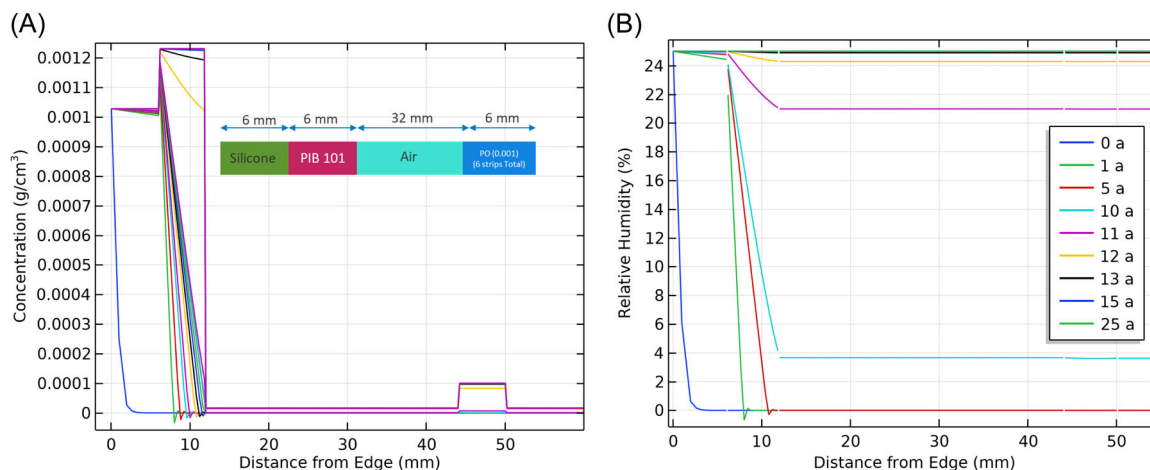


FIGURE 6 Model option #2, the discrete interlayer is as shown in Figure 4B, but with a PO matrix with 0.001 g/cm^3 , the concentration is plotted from the edge of the module to the center starting at a midpoint on the longer edge. (A) Concentration profile of mobile moisture. (B) Relative humidity (RH) profile, the legend in (B) shows the line color that corresponds to the year in the simulation.

This model has enough desiccant to absorb 0.001 g/cm^3 as compared to 0.032 g/cm^3 in PIB 101. In this case, the moisture is easily able to get into the ribbing keeping the RH in the air gap extremely low up through year 18 when the desiccant is spent, and the humidity rises very rapidly. Because there is a 10-year lag for water to get past the PIB 101 perimeter, the amount of desiccant in the PO is essentially capable of creating an ~ 8 -year delay. A doubling of the amount of desiccant should bring the time for the desiccant to be spent to approximately 25 years. The complexity of this finite element modeling is not needed to estimate how much desiccant is needed at a minimum. One can estimate a lag time and a steady state permeation rate through the perimeter PIB based on its geometry, and from there it is just a matter of calculating a total amount of desiccant in the center to absorb all the moisture for a given amount of time (Figure 6).

4.3 | Model #3

Model #3 is similar to Model #2, but with the desiccant loading in the PO set at 0.032 g/cm^3 as present in PIB 101. Or this is equivalent to Model #1 but with the ribbing matrix as a PO as opposed to a PIB. Here, it takes about 45 years for the ribs to become saturated. When compared to Model #1, the RH of the air is much lower, demonstrating the need to have a high diffusivity matrix holding the desiccant enabling it to be more easily utilized when its function is to absorb moisture in the package as opposed to blocking entry (Figure 7).

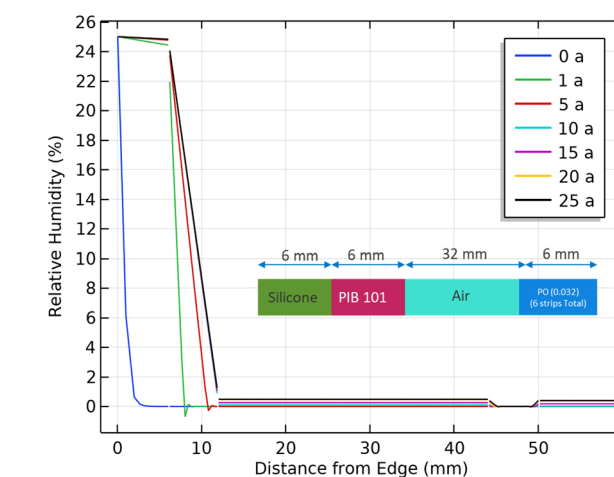


FIGURE 7 Model option #3, the discrete interlayer is as shown in Figure 4B, but with a PO matrix with 0.032 g/cm^3 . The relative humidity is plotted from the edge of the module to the center starting at a midpoint on the longer edge over the course of 25 years.

4.4 | Model #4

In this model, the number of ribs in the center area is increased from 6 (in Model #1) to 11, which more closely replicates the design used for Abound Solar modules.^{2,3} The intent is to see what the addition of more PIB ribbing can do. This change decreased the 25-year RH in the air from 1.45% down to 0.48%. This happens because the amount of perimeter area of the ribbing is doubled, but essentially the same amount of water diffuses in from the sides. This decreases the width of the spent desiccant in the ribbing by about a factor of two which effectively doubles the concentration gradient (or driving force for

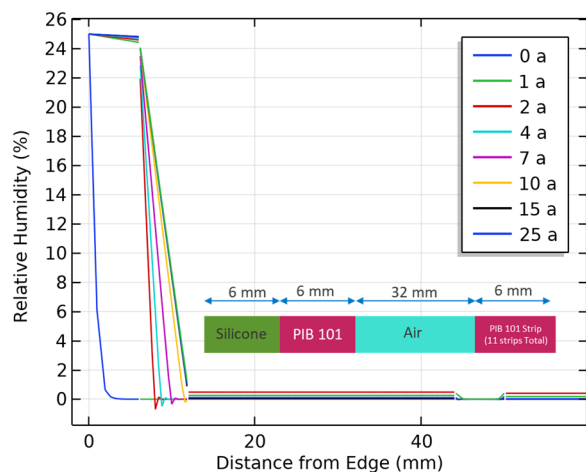


FIGURE 8 Model #4 relative humidity over 25 years. This model utilizes 11 polyisobutylene (PIB) 101 ribs, a 6-mm silicone and a 6-mm PIB 101 perimeter.

diffusion) by a factor of two for the same concentration in the air. If the perimeter is doubled and the diffusion length is decreased by a factor of two, the ability of the ribs to absorb water is increased by a factor of 4, which decreases the necessary humidity in the air gap by a factor of 4. Thus, the humidity in the air gap (RH_{air}) varies inversely as approximately the square of the ribbing perimeter length (l_{pr}) as

$$RH_{\text{air}} \sim \frac{1}{l_{\text{pr}}^2}. \quad (9)$$

If one were to use the same amount of material in the center region, but organized into thinner and more abundant ribs, the RH exposure can be significantly reduced with minimal cost increases (Figure 8).

4.5 | Model #5

In Model #5, the interlayer is simply filled with the PO polymer that does not contain a desiccant. It is difficult to extrude the PO all the way up to the PIB perimeter with sufficient precision that when pressed together, the PO will not extend over the PIB, making it ineffective. Therefore, as a worst-case scenario, a 2-mm air gap was modeled between the PIB and the PO, as in Figure 4C, but with a 2-mm instead of a 2-cm air gap.

As with the other models utilizing a 6-mm PIB 101 perimeter seal, there is a 10-year delay in moisture ingress. But in this model design, the PO will simply approach saturation over the 25-year time frame (Figure 9). For a moisture-sensitive material, this will

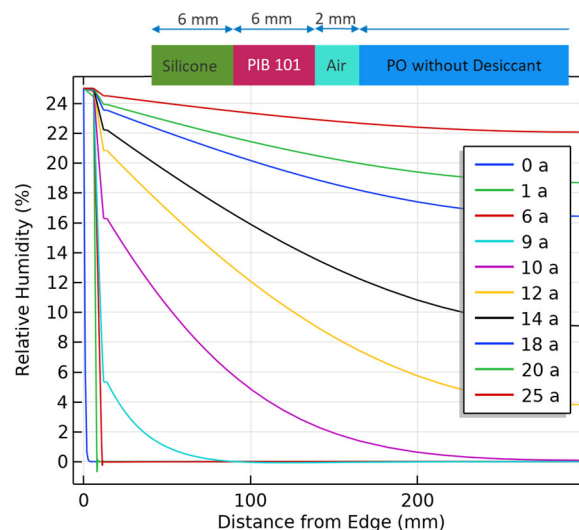


FIGURE 9 Relative humidity profile progress of Model #5 utilizing a 6-mm silicone, 6-mm polyisobutylene (PIB) 101 perimeter, and 2-mm air perimeter sequence with a PO interlayer without desiccant. This model is similar to Figure 4C, but with a 2-mm air gap.

not be acceptable, but with a moisture-resistant Si-based technology, there would still be a substantial reduction in exposure to moisture. Furthermore, in a dryer or cooler environment, the 6-mm edge seal may be sufficient by itself. As is, this design would likely be adequate for less moisture-sensitive technologies.

4.6 | Model #6

Model #6 is similar to Model #5, but with a desiccant capable of absorbing 0.0001 g/cm^3 of moisture in the PO interlayer. This amount of desiccant is small enough that even if placed in front of the cells, the loss of power due to light scattering would be insignificant and lower than the uncertainty of the module performance measurements. The addition of a desiccant would affect the apparent diffusivity and would add in a reversible component to moisture adsorption on the desiccant particles, but for the purposes of this study, we are ignoring these effects. Furthermore, this is just a theoretical typical PO, so precision in its properties is not useful.

This amount of desiccant is sufficient to prevent moisture from reaching the center of the module for about 10 years after it gets through the edge seal (Figure 10). This design will further reduce the moisture exposure, but over the life of the module, there will still be significant exposure to water.

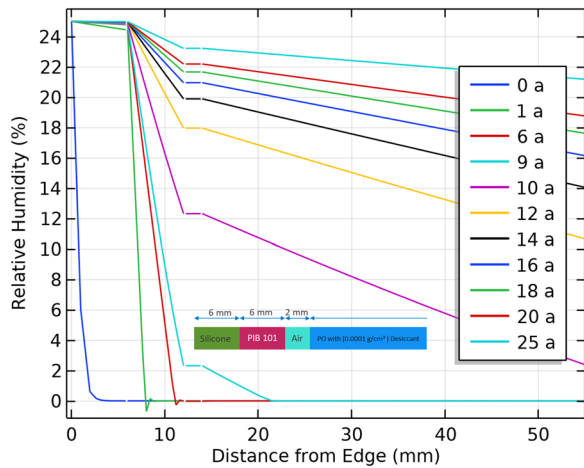


FIGURE 10 Relative humidity profile progress over 25 years of Model #6 utilizing a 6-mm silicone, 6-mm polyisobutylene (PIB) 101 perimeter, and 2-mm air perimeter sequence with a PO interlayer containing desiccant capable of absorbing 0.0001 g/cm^3 water. This model is similar to Figure 4C, but with a 2-mm air gap and desiccant in the PO layer.

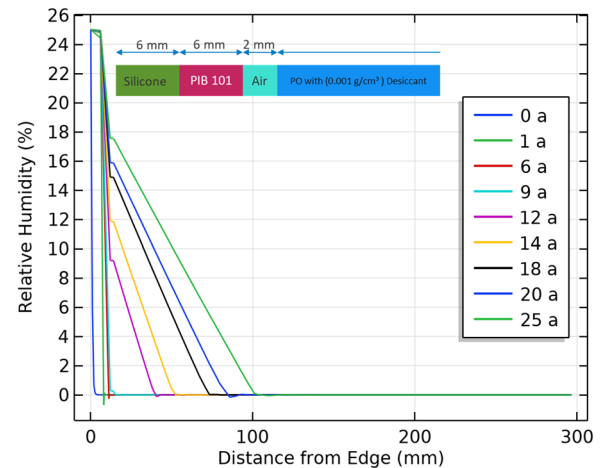


FIGURE 11 Relative humidity profile progress of Model #7 utilizing a 6-mm silicone, 6-mm polyisobutylene (PIB) 101 perimeter, and 2-mm air perimeter sequence with a PO interlayer containing desiccant capable of absorbing 0.001 g/cm^3 water $10\times$ more than Model #6. This model is similar to Figure 4C, but with a 2-mm air gap and desiccant in the PO layer.

4.7 | Model #7

Model #7 is similar to Model #5, but with a desiccant capable of absorbing 0.001 g/cm^3 of moisture that is $10\times$ more than Model #6. This larger amount of desiccant can limit moisture ingress to the perimeter of 100 mm over the course of 25 years. But this is still insufficient for a moisture-sensitive PV technology. Unless one is willing to accept moisture-induced degradation around the perimeter of a module, putting a desiccant throughout the interlayer is not adequate. Furthermore, at this loading, most of the desiccant would not be utilized (Figure 11).

4.8 | Model #8

Model #8 is similar to Model #6, but uses a PIB edge seal that does not have a desiccant in it. The primary difference between the results of the models is that it only takes a year instead of ~ 10 years for moisture to get through the edge seal (Figure 12). This makes the line at 16 years in Model #8 roughly equivalent to the line at 25 years in Model #6.

4.9 | Model #9

Model #9 is composed of 6 mm of silicone on the outer edge, 6 mm of PIB 107, a 2-mm-wide desiccated PO band, and PO without desiccant in the rest of the interlayer

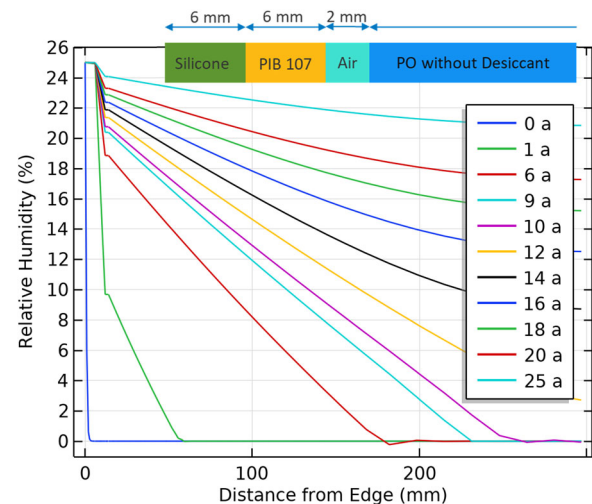
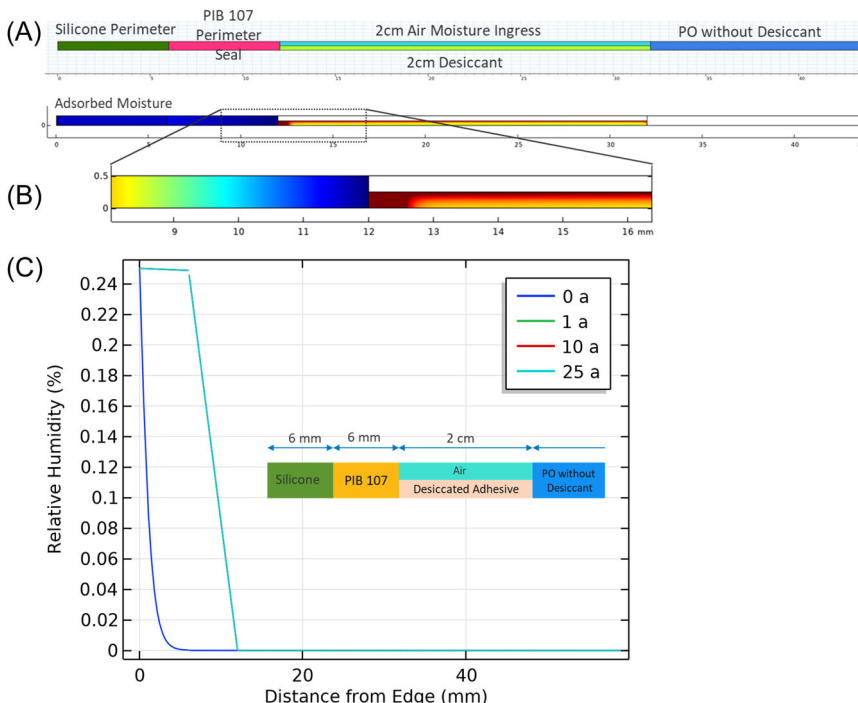


FIGURE 12 Relative humidity profile progress of Model #8 utilizing a 6-mm silicone, 6-mm polyisobutylene (PIB) 107 perimeter, and 2-mm air perimeter sequence with a PO interlayer containing desiccant capable of absorbing 0.0001 g/cm^3 water. This model is similar to Figure 4C, but with a 2-mm air gap and desiccant in the PO layer.

(Figure 4C). The 2-cm band of desiccated adhesive with an air gap on top is designed to allow for easy manufacturing in a way that the PO-desiccant layer is thinner than the PIB 107 layer and thus not likely to be squeezed over it. If this layer mixes with the nondesiccated PO interlayer, it will not cause issues. This air/desiccated PO section was modeled as air with $1/2$ the solubility and with desiccant able to absorb 0.05 g/cm^3 .

FIGURE 13 Model #9 (A) schematic composition. (B) Output from the *X-Z* plane model after 10 years of exposure. (C) Relative humidity (RH) versus distance from the side of the model with only 60 mm of the 60 cm total model, which is half the width of the module. The lines at 1 year and 10 years are hidden underneath the line at 25 years.



Because this section is not structurally important, the amount of desiccant can be much higher than this if desired and could even accommodate a desiccant that would expand as it absorbed moisture. The important aspect is the total amount of desiccant per length of perimeter. In this model, we used PIB 107 to demonstrate how effective this design is, but switching to PIB 101 would essentially shift the lag time till moisture got in by 9 or so years. The concept with this design is that the desiccant is far more effective if placed after the low diffusivity seal and it is similar to the number and loading of the ribbing in the other designs. The potential lifetime of this design can be easily modified by changing the amount of desiccant.

Because of the air gap, this model is really a 3D diffusion problem. However, if the moisture ingress distance is not far, then one can model it as a 2D model in the *X-Z* plane as opposed to the module in the *X-Y* plane, as has been the case for all previous discussions. This is essentially modeling the module as being 60 cm wide and infinitely long (Figure 13).

Here we see that after 25 years, the desiccant is still viable and capable of keeping the moisture out for a long time (Figure 13C). In this simulation, the moisture only reaches a value of 0.07% in the interlayer area, but reaching 0.068% in about 10 years and not rising much after that. This steady-state value is very low and is very sensitive to modeling parameters; therefore, the actual value should be regarded as within the noise of the modeling error. Even with an air gap in this region, this

design is able to keep the moisture level almost at ~0% for the life of a module.

This model is a worst-case scenario of this design concept. It should not be too difficult to reduce or eliminate the air gap or to have the air gap as one or two 1-mm-wide bands in the edge structure. The primary design factor with this concept is to tailor the amount of desiccant per length of the perimeter to the design lifetime and environment of the module.

4.10 | Model #10

Because of how the interlayer is extruded onto the glass plates, it is possible to place edge seal material directly in the vicinity of the J-box feedthrough hole in a module, shown in Figure 14A. This will not protect the area directly behind the J-box, but if the degradation does not cause a cell to be shunted or to go into reverse bias, the effect will be minimal. A small area with reduced voltage or higher series resistance resulting from moisture degradation would have a minimal overall effect. The presence of this J-box hole functions like a small increase in the perimeter and has a negligible effect on the overall moisture ingress as compared to Model #1, which is otherwise the same. For Model #9, a similar J-box design would include a 6-mm PIB 107 and a 2-cm desiccant fill PO annular region and would similarly not be expected to affect the overall moisture ingress protection.

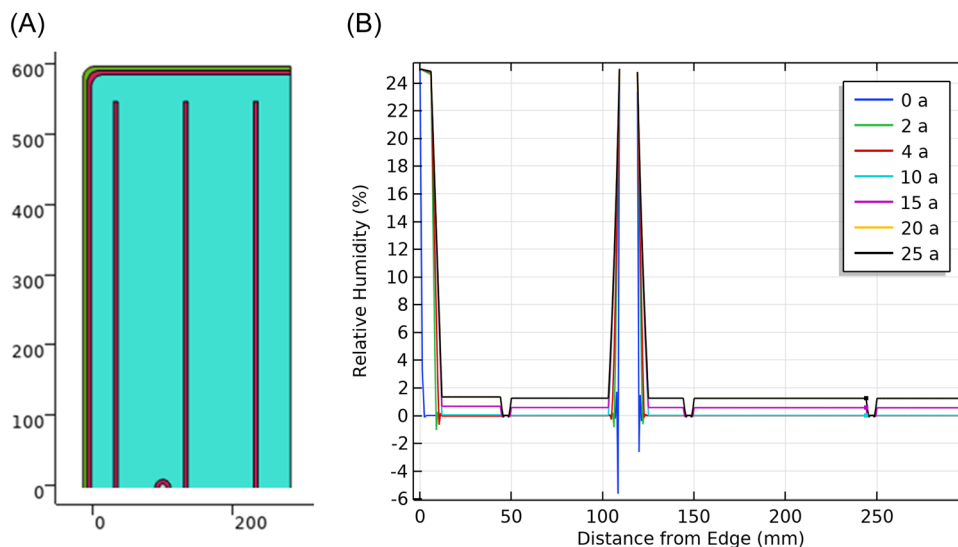


FIGURE 14 Model #10. Schematic of a module with a J-Box hole. This design is like Model #1, but with a 13-mm-diameter J-box hole with a 6-mm-wide edge seal polyisobutylene (PIB) 101 around it. (A) Schematic model used for Model #10 (B) output along the line at $y = 0$ cm.

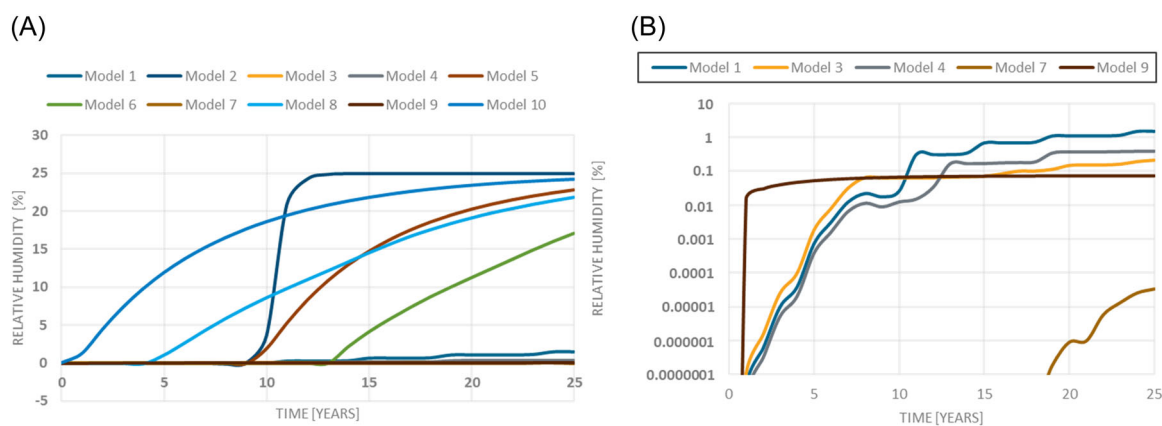


FIGURE 15 Progress of interior interlayer relative humidity versus time for the different design models. (A) All models. (B) Logarithmic plot of the best-performing models.

5 | DISCUSSION

To help succinctly visualize the moisture in the models as a function of time, the humidity in a position in the center of the modeled quadrant (Figure 4C) was plotted as a function of time (Figure 15). Models #1, 3, 4, 7, and 9 maintained an RH under 2% over 25 years in this center area. The models that did not work either had no desiccant or insufficient amounts of desiccant in the interlayer (2, 5, 6, 8, and 10). Model #7 appears to be successful, but as discussed above, it fails to protect the perimeter cells from moisture. This is because Figure 15 shows the concentration at a significant distance from the edge, such that with just a small amount of desiccant in a filled interlayer, this point is not affected by

moisture. Lastly, Models #1, 3, 4, and 9 do a really good job keeping the moisture exceptionally low at levels generally understood to be needed for many thin film technologies. The exact level needed is likely to vary between 10% and 0.01% for technologies based on amorphous Si, CdTe, CIGS, or perovskite materials. The package designs presented here can be tailored to any needed level of moisture protection.

It is also of interest to consider how much desiccant is used in the different designs, and how well it is utilized to keep moisture out. Desiccant costs more than other additives but is not so expensive that great efforts are needed to minimize its use. For a baseline, the amount of desiccant needed for a 25-year module can be estimated by ignoring the transient permeation in the perimeter

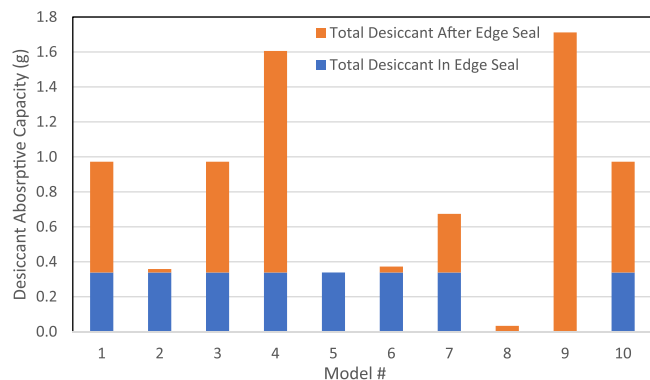


FIGURE 16 The amount of desiccant absorptive capacity in each of the models. Desiccant is differentiated as being either in the perimeter edge seal or in the interlayer. For this estimate, the thickness was assumed to be 0.5 mm.

and assuming a 6-mm perimeter of 0.5-mm-thick PIB 107. At 45°C and 25% RH, the permeability is 1.55×10^{-11} g/(cm s). For the 120 cm \times 60 cm module, this results in a total permeation rate of 4.66×10^{-10} g/s, which for 25 years is a total ingress mass of 0.37 g. In theory, the amount of desiccant in just the 6-mm perimeter PIB 101 is almost enough, but because it is distributed throughout the perimeter edge seal, the path length to the outside is on average half the length resulting in moisture breakthrough after only about 9 or 10 years. Alternatively, if PIB 101 is used at the perimeter, then the desiccant inside is only required to protect against an additional about 16 years, which is about 0.235 g of absorptive capacity after the edge seal. If Model #3 used PIB 101, did not have the air gap, and was designed to absorb 0.10 g/cm^3 of water, then the desiccant-filled PO layer would only have to be 0.1 mm wide. Model #9 used a much wider desiccated PO width and a much lower loading, but because this component is small and not relied upon for structural strength, it can easily be designed to absorb essentially all the moisture with a very small width (Figure 16).

Another consideration with Models #6 and #7 is that a much higher concentration of desiccant could be put in the back encapsulant only in the area between cells. With a Si wafer-based technology, this highly filled encapsulant would provide good back-scattering of light to be utilized on the front side and would enable the use of bifacial solar cells. Any residual bubbles or air gaps in the backside, or the overlap of the desiccant-filled encapsulant would have minimal effect on the module performance. It is much more important to get the front side encapsulant layer applied with minimal defects, which could be a single extruded film in this case, making the prospect more likely to be useful.

6 | CONCLUSIONS

The unique module interlayer and edge seal designs modeled here provide pathways to avoid vacuum lamination and significantly cut module assembly time to reduce capital expenditures. This is accomplished using hot melt extrusion to apply encapsulation edge seals and interlayer materials which further saves costs by avoiding the formation of encapsulant films. Keeping polymeric materials in either a pellet form and/or contained in drums, as opposed to rolls, can make materials handling more efficient too.

Model designs #1, #2, #3, #4, and #10 all use an interlayer composed primarily of air, but with ribbing interspersed to hold glass plates together. When a PIB-based material is used as the polymer matrix containing desiccant, the low diffusivity of PIB prevents the desiccant from being fully utilized, but which only results in the RH reaching a few percent (if enough desiccant is present). But if a high diffusivity material is used as the desiccant in the ribbing, all the desiccant is easily utilized over the 25-year expected lifetime of the module.

The use of extrusion for the application of the interlayer allows for desiccant-laden materials and/or low diffusivity PIB to be placed around the J-box hole, Model #10. This can easily be designed to provide 25 years of moisture protection in this area.

Model #9 presents the most effective use of desiccant. Here, the outer perimeter edge seal utilizes a PIB material, with or without desiccant in it. Then, the next band of material is a highly desiccant-loaded material. Considering that molecular sieve-based desiccants can only hold about 23% wt% moisture at saturation, a polymer matrix with ~50% loading would be needed to create a material capable of holding around 10 wt% water. Such a material would have exceptionally poor mechanical characteristics and might be difficult to extrude. But we show that even if air gaps are allowed, most of the water can be contained in a perimeter band of this material. Theoretically, less than a millimeter width of such a band would be necessary. This can also be interpreted as a way to augment a small-width edge seal by constructing it of two bands of material, the first of which is the diffusion barrier, and the second which is a small highly absorbing desiccated band.

ACKNOWLEDGMENTS

This project, Advanced Module Architecture for Reduced Costs, High Durability, and Significantly Improved Manufacturability, was funded by the Department of Energy Solar Energy Technologies Office under DE-EE-0008161 0. We would also like to acknowledge Josha

Morse for his help with transient water vapor transmission measurements used to determine permeation parameters.

ORCID

Michael D. Kempe  <http://orcid.org/0000-0003-3312-0482>

REFERENCES

- Peike C, Purschke L, Weiss K, Köhl M, Kempe M. Towards the Origin of Photochemical EVA Discoloration: 2013 IEEE 39th Photovoltaic Specialists Conference (PVSC), Tampa, FL, USA. IEEE; 2013:1579-1584.
- Barth KL. Production Ramping of Abound Solar's CdTe Thin Film Manufacturing Process: 37th IEEE Photovoltaic Specialists Conference, Seattle, WA, USA. IEEE; 2011:03394-03398.
- Barth KL, Hemenway D. Progress Toward Developing a Novel Module Architecture for Increased Reliability and Reduced Costs: 2014 IEEE 40th Photovoltaic Specialist Conference (PVSC). IEEE; 2014:0166-0169.
- Saint-Sernin E, Einhaus R, Bamberg K, Panno P. Industrialisation of Apollon's Nice Module Technology: 23rd European Photovoltaic Solar Energy Conference and Exhibition, 1 January 2008, Valencia, Spain. WIP Munich; 2008.
- Einhaus R, Bamberg K, Franclieu R, Lauvray H. New Industrial Solar Cell Encapsulation (NICE) Technology for PV Module Fabrication at Drastically Reduced Costs: 19th European Photovoltaic Solar Energy Conference. 2004.
- Madon F, Einhaus R, Degoulange J, Comparotto C, Galbiati G, Wefringhaus E. Bifacial NICE modules from high efficiency n-type BiSoN solar cells. *Energy Procedia*. 2015;77:382-385.
- Couderc R, Amara M, Degoulange J, Madon F, Einhaus R. Encapsulant for glass-glass PV modules for minimum optical losses: gas or EVA? *Energy Procedia*. 2017;124:470-477.
- Ellis S, Maple L, Shimpi T. Demonstration of Non-Lamination Encapsulation Techniques for Thin Film Solar Modules: 47th IEEE Photovoltaic Specialists Conference (PVSC), Calgary, Canada, 14 June 2020. Institute of Electrical and Electronics Engineers Inc.; 2020:1924-1926.
- Barth KL, Morgante J, Sampath WS, Shimpi TM. Progress Towards a Non-Lamination Encapsulation Technology to Improve Reliability and Reduce Costs: 2019 IEEE 46th Photovoltaic Specialists Conference (PVSC), Seattle, WA, USA. IEEE; 2019:0495-0498.
- Wohlgemuth J. Long Term Photovoltaic Module Reliability: NCPV and Solar Program Review Meeting, Denver, CO, NREL/CD-520-33586. National Renewable Energy Laboratory; 2003:183-179.
- Jordan DC, Kurtz SR. Photovoltaic degradation rates—an analytical review: photovoltaic degradation rates. *Prog Photovoltaics Res Appl*. 2013;21(1):12-29.
- Coyle DJ. Life prediction for CIGS solar modules part 1: modeling moisture ingress and degradation. *Prog Photovoltaics Res Appl*. 2011;21(2):156-172.
- Coyle DJ, Blaydes HA, Northey RS, et al. Life prediction for CIGS solar modules part 2: degradation kinetics, accelerated testing, and encapsulant effects. *Prog Photovoltaics Res Appl*. 2011;21(12):173-186.
- Visoly-Fisher I, Dobson KD, Nair J, Bezalel E, Hodes G, Cahen D. Factors affecting the stability of CdTe/CdS solar cells deduced from stress tests at elevated temperature. *Adv Funct Mater*. 2003;13(4):289-299.
- Malmström J, Wennerberg J, Stolt L. A study of the influence of the Ga content on the long-term stability of Cu(In,Ga)Se₂ thin film solar cells. *Thin Solid Films*. 2003;431-432:436-442.
- Quintana MA, King DL, McMahon TJ, Osterwald CR. Commonly Observed Degradation in Field-Aged Photovoltaic Modules (in English): 27th IEEE Photovoltaic Specialist Conference Program, New Orleans, LA, 19-24 May 2002. IEEE; 2002:1439-1436.
- Kempe MD, Terwilliger KM, Tarrant D. Stress Induced Degradation Modes in CIGS Mini-Modules: 33rd IEEE Photovoltaic Specialist Conference Program, San Diego, CA, 11-16 May 2008. IEEE; 2008.
- Kim Y, Kim H, Graham S, Dyer A, Reynolds JR. Durable polyisobutylene edge sealants for organic electronics and electrochemical devices. *Sol Energy Mater Sol Cells*. 2012;100:120-125.
- Cheacharoen R, Boyd CC, Burkhard GF, et al. Encapsulating perovskite solar cells to withstand damp heat and thermal cycling. *Sustain Energy Fuels*. 2018;2(11):2398-2406. doi:10.1039/C8SE00250A
- Kempe MD, Dameron AA, Reese MO. Evaluation of moisture ingress from the perimeter of photovoltaic modules. *Prog Photovoltaics Res Appl*. 2013;22(11):1159-1171. doi:10.1002/pip.2374
- Kempe MD, Nobles DL, Postak L, Calderon JA. Moisture ingress prediction in polyisobutylene-based edge seal with molecular sieve desiccant. *Prog Photovoltaics Res Appl*. 2018;26(2):93-101.
- Kempe MD, Panchagade D, Reese MO, Dameron AA. Modeling moisture ingress through polyisobutylene-based edge-seals. *Prog Photovoltaics Res Appl*. 2015;23(5):570-581.
- Lundberg JL, Mooney EJ, Rogers CE. Diffusion and solubility of methane in polyisobutylene. *J Polym Sci Part A-2*. 1969;7(5):947-962.
- Crank J. *The Mathematics of Diffusion*. Oxford Science Publications; 1975.
- Hanoka J, inventors; Evergreen Solar Inc., assignee. Frameless photovoltaic module. US patent 2008/0041442A1, 21 February 2008. 2008.
- Dow Corning Corp. *Develop Silicone Encapsulation Systems for Terrestrial Silicon Solar Arrays DOE/JPL/954995-80/6*. Dow Corning Corp; 1979.
- McIntosh KR, Cotsell JN, Cumpston JS, Norris AW, Powell NE, Ketola BM. An Optical Comparison Of Silicone and EVA Encapsulants for Conventional Silicon PV modules: A Ray-Tracing Study: 2009 34th IEEE Photovoltaic Specialists Conference 7-12 June 2009, Philadelphia, PA. IEEE; 2009:000544-000549.
- McIntosh KR, Powell NE, Norris AW, Cotsell JN, Ketola BM. The effect of damp-heat and UV aging tests on the optical properties of silicone and EVA encapsulants. *Prog Photovoltaics Res Appl*. 2011;19(3):294-300.
- Ketola BM, McIntosh KR, Norris AW, Tomalia MK. *Silicones for Photovoltaic Encapsulation*. 23rd European Photovoltaic Solar Energy Conference, 1-5 September 2008, Valencia, Spain. WIP Munich; 2008.

30. Terreau C, Habimana J, Jenkins S, inventors; Dow Silicones Corp, assignee. Encapsulation of solar cells. US patent 8847063B2, 30 September 2014. 2014.
31. Kempe M, Wohlgemuth J, Miller D, Postak L, Booth D, Phillips N. Investigation of a wedge adhesion test for edge seals. In: Kempe MD, Wohlgemuth JH, Miller DC, Postak L, Booth D, Phillips NH, eds. *SPIE Optics + Photonics for Sustainable Energy*. Vol. 9938. SPIE; 2016.
32. Kempe M, Korkmaz K, Postak L, Booth D. Using a butt joint test to evaluate photovoltaic edge seal adhesion. *Energy Sci Eng*. 2019;7(2):354-360. doi:10.1002/ese3.273
33. Kempe MD, Miller DC, Wohlgemuth JH, et al. Multi angle laser light scattering evaluation of field exposed thermoplastic photovoltaic encapsulant materials. *Energy Sci Eng*. 2016;4(1): 40-51. doi:10.1002/ese3.106
34. Kempe MD. A Field Evaluation of the Potential for Creep in Thermoplastic Encapsulant Materials: 2012 38th IEEE Photovoltaic Specialists Conference. IEEE; 2012:001871-001876.
35. Kempe M. Modeling of rates of moisture ingress into photovoltaic modules. *Sol Energy Mater Sol Cells*. 2006;90(16): 2720-2738.

How to cite this article: Kempe MD, Watts A, Shimpi T, Ellis S, Barth K. Modeling of the effectiveness of novel edge seal designs for fast, low-Cap-Ex manufacturing. *Energy Sci Eng*. 2023;11:2314-2329. doi:10.1002/ese3.1455